

UCSF

UC San Francisco Previously Published Works

Title

Programmed Cell-to-Cell Variability in Ras Activity Triggers Emergent Behaviors during Mammary Epithelial Morphogenesis

Permalink

<https://escholarship.org/uc/item/8bw3k20h>

Journal

Cell Reports, 2(5)

ISSN

2639-1856

Authors

Liu, Jennifer S
Farlow, Justin T
Paulson, Amanda K
[et al.](#)

Publication Date

2012-11-01

DOI

10.1016/j.celrep.2012.08.037

Peer reviewed



Published in final edited form as:

Cell Rep. 2012 November 29; 2(5): 1461–1470. doi:10.1016/j.celrep.2012.08.037.

Programmed Cell-to-Cell Variability in Ras Activity Triggers Emergent Behaviors during Mammary Epithelial Morphogenesis

Jennifer S. Liu^{1,2}, Justin T. Farlow^{1,3}, Amanda K. Paulson^{1,4}, Mark A. Labarge⁵, and Zev J. Gartner^{1,2,3,4,*}

¹Department of Pharmaceutical Chemistry, University of California, San Francisco, San Francisco, CA 94158, USA

²Chemistry and Chemical Biology Graduate Program, University of California, San Francisco, San Francisco, CA 94158, USA

³Tetrad Graduate Program, University of California, San Francisco, San Francisco, CA 94158, USA

⁴Biomedical Sciences Graduate Program, University of California, San Francisco, San Francisco, CA 94158, USA

⁵Life Science Division, Lawrence Berkeley National Laboratory, Berkeley, CA 94720, USA

SUMMARY

Variability in signaling pathway activation between neighboring epithelial cells can arise from local differences in the microenvironment, noisy gene expression, or acquired genetic changes. To investigate the consequences of this cell-to-cell variability in signaling pathway activation on coordinated multicellular processes such as morphogenesis, we use DNA-programmed assembly to construct three-dimensional MCF10A microtissues that are mosaic for low-level expression of activated H-Ras. We find two emergent behaviors in mosaic microtissues: cells with activated H-Ras are basally extruded or lead motile multicellular protrusions that direct the collective motility of their wild-type neighbors. Remarkably, these behaviors are not observed in homogeneous microtissues in which all cells express the activated Ras protein, indicating that heterogeneity in Ras activity, rather than the total amount of Ras activity, is critical for these processes. Our results directly demonstrate that cell-to-cell variability in pathway activation within local populations of epithelial cells can drive emergent behaviors during epithelial morphogenesis.

INTRODUCTION

The behavior of an epithelial cell is strongly influenced by signals from the microenvironment. Many of these signals activate pathways downstream of the small GTPase Ras that affect behaviors including cell motility, survival, and proliferation. However, neighboring epithelial cells in the same tissue may differ substantially in their levels of Ras pathway activation as a consequence of local fluctuations in the

© 2012 The Authors

*Correspondence: zev.gartner@ucsf.edu.

SUPPLEMENTAL INFORMATION

Supplemental Information includes Extended Experimental Procedures, four figures, and four movies and can be found with this article online at <http://dx.doi.org/10.1016/j.celrep.2012.08.037>.

LICENSING INFORMATION

This is an open-access article distributed under the terms of the Creative Commons Attribution-Noncommercial-No Derivative Works 3.0 Unported License (CC-BY-NC-ND; <http://creativecommons.org/licenses/by-nc-nd/3.0/legalcode>).

microenvironment, stochastic events, or acquired genetic and epigenetic changes. The resulting cell-to-cell variability may lie dormant or trigger regulatory pathways that act at the level of cell communities to direct collective cell behaviors (Vitorino and Meyer, 2008), remove cellular defects from a tissue (Eisenhoffer et al., 2012; Takemura and Adachi-Yamada, 2011), or drive malignancy (Hogan et al., 2009; Leung and Brugge, 2012; Marusyk et al., 2012).

In vitro culture of epithelial cells can facilitate the study of cell-to-cell variability by providing tight control of the cellular microenvironment. However, three-dimensional (3D) culture in laminin-rich extracellular matrix (lrECM) is required to reveal the consequences of cell-to-cell variability on collective cell behaviors such as epithelial morphogenesis. Under these 3D culture conditions, single MCF10A breast epithelial cells proliferate to form polarized microtissues that ultimately growth arrest as multicellular acini. These small tissues recapitulate important structural and functional features of the organ from which they were derived (Streuli et al., 1991) and even exhibit cell-to-cell variability in the activation level of kinases downstream of Ras, such as Akt, Erk, and MLCK (Debnath et al., 2002; Pearson and Hunter, 2009; Yuan et al., 2011). Unfortunately, directly analyzing the consequences of such cell-to-cell variability in Ras pathway activation within 3D cultured tissues is challenging, due in part to the difficulty of efficiently and selectively altering this signaling node in specific cells with both high temporal and spatial precision.

Several methods are suitable for preparing tissues mosaic for activated proteins such as Ras. Optogenetic techniques offer exceptional precision but are generally low throughput and require significant engineering of the protein or process of interest (Wang et al., 2010). Currently, the best general solutions involve mixing two or more cell populations (Mori et al., 2009; Hogan et al., 2009) or infection of tissues by low-titer virus (Leung and Brugge, 2012; Lu et al., 2008). However, the resulting mosaic tissues span a distribution of compositions, where only a fraction of the microtissues possess the desired numbers of each cell type for subsequent analysis. These configurational inconsistencies complicate the quantification of rare events and processes that occur rapidly upon the initiation of cell-cell interactions. We therefore sought an alternative method for preparing epithelial microtissues mosaic for H-Ras activity that provides additional control over initial aggregate composition and cell-to-cell connectivity, thereby facilitating quantitative analysis and increasing the time resolution of experiments involving dynamic cellular interactions during the early stages of epithelial morphogenesis.

Here, we report DNA-programmed assembly as an approach for building mosaic epithelial microtissues with defined cell-to-cell variability for 3D culture. We demonstrate that cell aggregates of wild-type (WT) MCF10A epithelial cells prepared by programmed assembly rapidly condense into polarized microtissues in 3D culture. We then use this method to analyze interactions between neighboring cells with subtle differences in Ras activation during the early stages of morphogenesis. We find that whereas low-level and chronic activation of H-Ras is insufficient to disrupt morphogenesis in microtissues homogeneously expressing a constitutively active form of the gene, the same level of Ras activation in only subsets of cells leads to the emergence of distinct phenotypes specifically in mosaic microtissues. Our results directly demonstrate that slight biochemical or genetic differences between neighboring cells can give rise to unique and emergent behaviors in epithelial tissues (Altschuler and Wu, 2010).

RESULTS

Programmed Assembly Generates MCF10A Aggregates with Defined Size and Cellular Composition for 3D Culture

To build mosaic 3D epithelial microtissues with defined composition, we applied a programmed assembly strategy. Although the use of programmed assembly has previously been used to build aggregates of six to ten cells, these aggregates were constructed using suspension or loosely adherent cell lines (Gartner and Bertozzi, 2009). Therefore, it was not known whether a similar protocol would label and direct the assembly of tightly adherent epithelial cells such as the MCF10A or MDCK lines. More importantly, it was not clear whether chemically assembled epithelial cells would integrate into a coherent and polarized microtissue under typical 3D culture conditions. We therefore first sought to establish the broad applicability of programmed assembly by combining populations of epithelial cells expressing different fluorescent proteins into controlled aggregates for 3D culture (Figure 1A).

For the programmed assembly of cell aggregates mosaic for fluorescent protein expression, MCF10A cells expressing H2B-RFP or H2B-GFP were first prepared as single-cell suspensions by treatment of monolayer cultures with EDTA followed by a brief pulse with low-concentration trypsin. We then chemically modified a fraction of MCF10A cell surface lysines with 20-base oligonucleotides bearing a reactive NHS-ester functionality at their 5' ends (Hsiao et al., 2009; Selden et al., 2012) (Figure 1A). These DNA-conjugated cells were imparted with selective adhesive properties, yet retained the same viability and proliferative capacity as unmodified cells (Figure S1A). We initiated programmed assembly by mixing populations of green- and red-fluorescent MCF10A cells bearing complementary strands on their cell surfaces at a 1:50 ratio to prevent the red cells from reacting with more than one green cell. Fluorescence microscopy of the crude assembly reaction revealed a population of uniform cell aggregates composed of a single green cell surrounded by four to six red cells in addition to excess unassembled red cells (Figure 1B). No aggregation was observed upon mixing of unlabeled cells or cells labeled with mismatched DNA strands (Figure S1B). The Madin-Darby canine kidney (MDCK) epithelial cell line could similarly be assembled when labeled with lipid-modified oligonucleotides (Figure S1B) (Selden et al., 2012).

To quantify the efficiency of the self-assembly process, we analyzed aggregates by flow cytometry. Greater than 95% of the green cells assembled with red cells when bearing matched cell surface oligonucleotides, compared with only 5% in unlabeled or mismatched DNA-labeled cells (Figure S1C). Fluorescence-activated cell sorting (FACS) was used to remove excess red cells and prepare enriched populations of mosaic MCF10A and MDCK aggregates for 3D culture (Figures 1C and S1D). A total of 5,000–10,000 aggregates were routinely sorted directly onto IrECM-coated chamber slides where they rapidly condensed into spherical 3D microtissues with phase-dense boundaries over 6–12 hr (Figures 1D and S1E). Time-lapse imaging of fluorescently labeled cell nuclei during this process revealed a transition from a disordered aggregate to a spherical microtissue with symmetrically arranged nuclei over a similar time frame (Figure 1E). Consistent with previous reports of MCF10A morphogenesis beginning from single cells, morphogenesis of microtissues formed by the programmed assembly process involved considerable cell motility (Ferrari et al., 2008; Pearson and Hunter, 2007; Tanner et al., 2012). These cell movements also became more concerted and continued at later time points (Movie S1).

Acquisition of Microtissue Polarity in Chemically Assembled MCF10A Cells Occurs within 12 hr in 3D Culture

The observation that multicellular aggregates are motile and rapidly condense suggested that the cells were polarizing and replacing their DNA-based chemical adhesions with native-like, protein-based adhesions. To determine whether aggregates were indeed polarizing during the first 24 hr in culture, we performed indirect immunofluorescent staining for protein localization at regular intervals after programmed assembly and purification by FACS. Immediately after sorting of MCF10A aggregates, hemidesmosomal adhesion molecule α_6 -integrin and adherens junction protein β -catenin were localized to individual cell edges, whereas *cis*-Golgi protein GM130 was randomly oriented relative to cell nuclei (Figures 2A and S2A). These results indicate that cells remained distinct entities immediately after programmed assembly despite their DNA-based chemical adhesions. By 12 hr after assembly these markers for cell polarity were enriched at appropriate subcellular locations (Figures 2A and 2B). By 24 hr, protein localization was pronounced; β -catenin was enriched at cell-cell interfaces, α_6 -integrin was enriched at the basolateral surface of the microtissue, and GM130 was apically localized relative to cell nuclei (Figures 2A, 2B, and S2A). Additional staining of microtissues 24 hr after assembly revealed basal deposition of laminin-5 and actin enrichment at the cell cortex (Figure 2C). These staining patterns indicate that cell aggregates rapidly condense into polarized microtissues and are consistent with staining patterns of developing microtissues of similar size grown from single cells after 4 days in culture (Debnath et al., 2002) (Figures 2A and S2A). Polarity was also maintained at later time points (Figures S2B and S2C).

In addition to acquisition of tissue-level polarity, epithelial morphogenesis is marked by growth arrest followed by lumen formation after extended 3D culture (Debnath et al., 2002). Up to 96 hr after assembly, the majority of assembled microtissues were uniformly positive for the proliferation marker Ki-67 (Figures 2D and 2E). However, microtissues were largely negative for Ki-67 at later time points. Moreover, cells positive for cleaved caspase-3 in the clearing luminal space, which were largely absent at 24 hr, became evident as early as 96 hr and were present in nearly all acini by day 16 (Figures 2D and 2E).

To test the applicability of this approach for generating other epithelial microtissues, we evaluated the polarity and lumenogenesis of MDCK aggregates in 3D culture after programmed assembly. MDCK cells undergo lumenogenesis by a different mechanism than MCF10A cells, providing an additional test for the compatibility of programmed assembly with diverse cellular processes during morphogenesis. MDCK aggregates grown for 6–7 days in IrECM were uniformly polarized as judged by staining for apical marker gp135 and β -catenin (Figure 2F, left). Developing lumens were also observed, consistent with previous reports of MDCK cysts grown from aggregates (Liu et al., 2007). Additionally, the morphology of cysts was similar to the morphology of cysts of equivalent size grown from single cells (Figure 2F, right). Combined, these data indicate that the hallmarks of epithelial morphogenesis—polarity, growth arrest, and lumen formation—are recapitulated when epithelial cell aggregates prepared by programmed assembly are grown in 3D IrECM culture.

MCF10A^{Ras} Cells Undergo Morphogenesis Similar to MCF10A^{WT} Cells

To understand how groups of cells undergoing morphogenesis respond to cell-to-cell variability in Ras activation within the same tissue, we required a MCF10A derivative cell with modestly elevated Ras activity but also with basic epithelial character and the ability to interact with neighboring WT cells. Ras pathway activation in an ideal MCF10A derivative should be elevated but consistent with levels observed in normal tissues. However, we found that cells expressing H-Ras^{V12} under the control of the strong Moloney murine leukemia

virus LTR had very high levels of Ras expression and Erk phosphorylation, lost E-cadherin expression and their epithelial morphology after a few passages, and formed highly invasive and disorganized structures in 3D culture (Figures 3B and S2D; Movie S2) (Elenbaas et al., 2001). Therefore, MCF10A cells over-expressing H-Ras^{V12} were a poor choice for modeling heterogeneous Ras activation during normal physiological processes.

In contrast the MCF-10AneoT cell line (referred to here as MCF10A^{Ras} for clarity) retained its epithelial characteristics despite chronic H-Ras activation. These cells were generated by stable transfection with a mutant *Ras* gene encoding the constitutively active H-Ras^{V12} protein (Basolo et al., 1991). Unlike acutely transduced cells, however, MCF10A^{Ras} cells were previously shown to express only a modest 4-fold increase in H-Ras and a 3- to 6-fold increase in phospho-Akt relative to MCF10A^{WT} (Kim et al., 2009). We confirmed these results and also observed a modest increase in phospho-Erk (Figure 3A). Additionally, MCF10A^{Ras} cells were found to express nearly WT levels of E-cadherin (Figure 3A). Consistent with their modestly elevated H-Ras activity, MCF10A^{Ras} cells formed acini that were larger in size than MCF10A^{WT} acini but still lumenized when grown from single cells for 23 days in 3D culture (Figure 3B). Similar to MCF10A^{WT} aggregates, assembled aggregates of MCF10A^{Ras} cells condensed into polarized microtissues over 24 hr (Figures 3C and S2E). After 16 days in 3D culture, they formed acini that were largely negative for Ki-67 but contained cells positive for cleaved caspase-3 in the lumen (Figures 3D and S2F). We therefore used MCF10A^{Ras} cells for building heterogeneous microtissues in subsequent experiments because they remained epithelial in character and displayed levels of Ras pathway activation consistent with normal tissues.

Single MCF10A^{Ras} Cells Lead Motile Multicellular Protrusions or Basally Extrude from WT Microtissues

Using programmed assembly, we prepared mosaic aggregates comprising a single MCF10A^{Ras} cell surrounded by WT cells. Although homogeneous aggregates of MCF10A^{Ras} cells were phenotypically similar to WT aggregates with respect to polarity and morphology over 24 hr, we unexpectedly observed emergent phenotypes in heterogeneous microtissues. In some cases, multicellular protrusions tipped by a single, motile MCF10A^{Ras} cell seemed to direct the motion of the surrounding WT microtissue across the IrECM over several hours (Figure 4A; Movies S3 and S4). Multicellular protrusions occurred in 20%–30% of the mosaic microtissues. In an additional 20%–30% of mosaic aggregates, we observed cell extrusion where the single MCF10A^{Ras} cell exited at the basal surface but remained loosely associated with the microtissue. Significantly, the multicellular protrusion and basal extrusion phenotypes were rarely observed for single MCF10A^{Ras} cells grown within homogeneous MCF10A^{Ras} microtissues (Figure 4B; Movie S3). These behaviors were not due to adaptation to chronic Ras activation, as they were also observed in heterogeneous assemblies made with single MCF10A cells acutely expressing H-Ras^{V12} (Figure S2G and Movie S2). Additionally, in 4%–6% of the mosaic aggregates, the MCF10A^{Ras} cell was highly motile and broke away from the surrounding WT microtissue, occasionally traversing over 100 μm (Figures S3A and S3B; Movie S4). Addition of high-activity DNase to the media immediately after sorting did not affect the frequency of extrusion and protrusions, indicating that DNA-based linkages between cells were not responsible for the observed phenotypes (Figure 4C).

Further characterization of heterogeneous microtissues revealed that both protruding and extruded cells were viable as judged by exclusion of a cell-impermeant DNA stain (Figure S3C). Protruding cells were often irregularly shaped with GM130 staining oriented away from the microtissue center (Figures S3D and S3E) but with strong staining for β -catenin at cell-cell adhesions with neighboring WT cells (Figure S3F). Basally extruded cells typically maintained a rounded morphology. We did not observe an actin ring in adjacent cells or any

unusual actin staining in extruded cells (Figure S3D). However, once fully extruded, cells did not exhibit β -catenin staining on membranes adjacent to the WT microtissue (Figure S3F). Because MCF10A^{WT} and MCF10A^{Ras} cells expressed similar levels of E-cadherin (Figure 4A) and were frequently observed to freely commingle, these behaviors could not be explained by differential E-cadherin expression alone (Movies S3 and S4). Moreover, heterogeneity, per se, was not responsible for the extrusion or multicellular protrusion phenotypes because single WT cells did not protrude or extrude from aggregates composed principally of MCF10A^{Ras} cells (Movie S3).

Ras activates multiple pathways in its GTP-bound form. PI3K and the MAPK signaling cascades have recently been implicated as important downstream effectors of analogous protrusive membrane activity and apical cell extrusions, respectively, during H-Ras^{V12} overexpression in confluent 2D MDCK monolayers and model organisms (Hogan et al., 2009). To determine whether these pathways were also necessary for basal cell extrusion and motile multicellular protrusions during heterogeneous MCF10A aggregate morphogenesis in IrECM, we treated freshly assembled mosaic aggregates with small-molecule inhibitors and quantified the distribution of resulting phenotypes over 24 hr in culture. Treatment with PI3K inhibitor LY294002 or PIK-90 reduced the formation of multicellular protrusions while slightly increasing the frequency of basal extrusions compared to treatment with DMSO control (Figures 4D, 4E, S3G, and S3H). In contrast, treatment of mosaic aggregates with the MEK inhibitor PD325901 or the Raf inhibitor Sorafenib blocked both multicellular protrusions and basal extrusions. The morphology of aggregates treated with inhibitors was indistinguishable from those treated with DMSO vehicle control (Figures S3I and S3J). Therefore, MEK activation was required for basal extrusions, whereas both PI3K and MAPK signaling pathways were necessary for motile multicellular protrusions.

Motility of MCF10^{Ras} Cells in Homogeneous and Heterogeneous Microtissues Is Quantitatively Different

To further characterize the emergent behaviors resulting from cell-to-cell variability in Ras activity, we tracked the positions of individual MCF10A^{WT} or MCF10A^{Ras} cells in microtissues over 24 hr. MCF10A^{WT} and MCF10A^{Ras} cells did not differ significantly in maximum displacement from their initial positions when grown within homogeneous microtissues containing only cells of the same type (Figures 5A and 5B). This is consistent with the qualitative observation that homogeneous microtissues have a normal morphology over this time period. In contrast the maximum displacement of single MCF10A^{Ras} cells in heterogeneous aggregates with surrounding WT cells was increased relative to the same cells in homogeneous MCF10A^{Ras} aggregates (Figures 5A and 5B) without a significant increase in average speed (Figure 5C). The increase in mean displacement of MCF10A^{Ras} cells when grown among MCF10A^{WT} cells was almost entirely attributable to microtissues with the multicellular protrusion phenotype (Figure 5D); when MCF10A^{Ras} cell tracks were segregated into normal, extruding, and protruding phenotypes, we found average displacements ($\pm 95\%$ CI) of 26 (± 3), 31 (± 5), and 61 (± 9) μm , respectively. Although the displacement of MCF10A^{Ras} cells in normal and extruding microtissues typically remained within the average diameter of heterogeneous microtissues (43.7 \pm 8.47 μm), the displacement of protruding cells generally exceeded the size of microtissues, sometimes significantly. To quantify the extent to which single, protruding MCF10A^{Ras} cells affected the motility of the surrounding WT microtissue, we compared the trajectories of the MCF10A^{Ras} cells to the trajectories of the surrounding microtissue. Overall, the trajectories for single MCF10A^{Ras} cells and their WT neighbors were correlated for all three phenotypes (Figure S4). Interestingly, the large displacements observed for single MCF10A^{Ras} cells participating in motile multicellular protrusions were also observed for their associated WT

microtissues (Figure 5E), indicating that the single MCF10A^{Ras} cell directs the motion of the entire microtissue. Moreover, subtracting the coordinates of the microtissue centroid from the coordinates of the protruding MCF10A^{Ras} cell generated residual trajectories (Figure 5E) that were qualitatively similar to those of single cells in homogeneous MCF10A^{Ras} and WT microtissues (Figure 5A). This analysis occasionally revealed residual trajectories with large total displacements, which always corresponded to the rare, hypermotile cells (Figure 5E, dashed orange track).

DISCUSSION

In order to study the consequences of cell-to-cell variability in Ras activation on the morphogenesis of MCF10A mammary epithelial cells in 3D culture, we used a chemical approach to assemble epithelial cell aggregates with programmed compositions, sizes, and initial cell-to-cell connectivities. The utility of our approach was 3-fold: (i) programmed assembly generated thousands of nearly identical microtissues, thus facilitating quantification of even rare phenotypes associated with cellular interactions among specific subpopulations; (ii) aggregate assembly was rapid and resulted in polarized microtissues within 12 hr in 3D culture, thus facilitating identification and characterization of phenotypes that emerged shortly after the initiation of cell-cell interactions; and (iii) the modularity of programmed assembly allowed the straightforward modification of microtissue composition to identify which cell populations, and in which proportions, contributed to emergent behaviors. Using this approach, we directly investigated the consequences of cell-to-cell variability in Ras activation during the morphogenesis of MCF10A epithelial cells. Remarkably, we found that even subtle variability in Ras activation between neighboring cells elicits emergent behaviors during epithelial morphogenesis, including basal cell extrusions and motile multicellular protrusions.

Epithelial cell extrusions that resemble those in our study are elicited under a variety of conditions. Cells overexpressing oncogenes such as ErbB2, Ras^{V12}, or v-Src have all been shown to extrude apically in confluent monolayer culture or growth-arrested mammary acini (Hogan et al., 2009; Kajita et al., 2010; Leung and Brugge, 2012). Cells undergoing apoptosis also extrude apically through the formation of a contractile actin ring in the surrounding cells (Rosenblatt et al., 2001) or basally upon disruption of microtubule regulation (Slattum et al., 2009). Recently, apical cell extrusions were shown to occur as a consequence of cell crowding and were proposed to contribute to tissue homeostasis (Eisenhoffer et al., 2012; Marinari et al., 2012). In this study we observed the extrusion of single MCF10A^{Ras} cells from within motile and growing MCF10A micro-tissues. In this dynamic 3D culture context, we found that cell extrusions occurred in the basal direction and did not appear to occur through the formation of a contractile actin ring as occurs during apoptosis.

The simplest explanation for the observed basal, as opposed to apical, extrusions was that the polarized microtissues in our study lacked a well-defined and clear luminal space. The availability of an unobstructed basal surface lacking tissue culture plastic or a mature basement membrane may also provide an opportunity for basal extrusion that was lacking in previous studies. Similar conditions may exist during the morphogenesis of the mammary gland in vivo and at the basal surface of carcinomas of a variety of tissues (Gjorevski and Nelson, 2011). Alternatively, the increased constriction of the microtissues at the apical surface or differences between epithelial cell lines used in the various studies may also explain the differences in the direction of extrusion. In any case, in certain in vivo contexts, basal extrusions occur more frequently than apical extrusions (Hogan et al., 2009; Shen and Dahmann, 2005). In MCF10A aggregates undergoing morphogenesis, basal extrusions of single MCF10A^{Ras} cells appeared to depend on MAPK but not PI3K pathway signaling.

Recently, Hogan et al. (2009) and Leung and Brugge (2012) observed a similar dependence on MEK during apical cell extrusions triggered by activation of Ras or ErbB2, respectively, suggesting that apical and basal extrusions in other systems may be related processes. However, the specific *in vivo* factors that determine the direction of cell extrusions will be important to identify because they may specify different fates for extruded cells in the context of development, homeostasis, or cancer.

In addition to basal extrusions, motile multicellular protrusions that were dependent on both PI3K and the MAPK signaling pathways were frequently observed in heterogeneous microtissues. Basal protrusions that are similarly sensitive to both MEK and PI3K inhibition have previously been observed during HGF-triggered tubulogenesis of MDCK cysts in 3D culture. HGF activates the Met receptor, which provides sustained activation of Ras similar to the ectopic expression of H-Ras^{V12} in our experiments (Khwaja et al., 1998; O'Brien et al., 2004). These behaviors may also play a role in angiogenesis and wound healing of endothelial cells (Graupera et al., 2008; Vitorino and Meyer, 2008). Motile multicellular protrusions are also analogous to border cell migration during *Drosophila* ovary development, where elevated growth factor receptor or Rac activation in single cells can drive collective cell motility of an entire cell aggregate (Inaki et al., 2012; Wang et al., 2010). Multicellular protrusions led by single cells may play a role during disease processes such as tumor progression and have been implicated in the invasive behaviors of cancers (Scott et al., 2010). Although invasion by multiple transformed cells in these diseased contexts is a well-appreciated phenomenon, the observation that single cells expressing oncogenic H-Ras^{V12} can drive the collective motility of nontransformed neighboring cells is surprising. Even more surprising is the fact that these multicellular protrusions, led by cells with only modestly elevated levels of activated Ras, are actually accentuated by the presence of neighbors with lower Ras activity. Similarly, we also observed an increased frequency of single MCF10A^{Ras} cells breaking away from the surrounding microtissue and rapidly traversing hundreds of microns in 3D culture when surrounded by WT cells. These observations are consistent with a growing body of work that indicates tumor cell dissemination is an early event in carcinoma progression *in vivo* (Hüsemann et al., 2008; Rhim et al., 2012; Weinberg, 2008). Moreover, they provide evidence that different modes of invasive behavior may coexist within the same tumor, where cellular heterogeneity is well documented (Friedl et al., 2012). Accordingly, our results may have significant implications for the initiation and progression of cancer.

In conclusion we have used a chemical-programmed assembly strategy to directly probe the consequences of cell-to-cell variability in Ras activation during the morphogenesis of MCF10A mammary epithelial cells in 3D culture. We find several emergent behaviors that occur as a consequence of modest differences in Ras activation between neighboring cells, rather than due to the absolute levels of Ras activation in the microtissue. Remarkably, the microtissues exhibiting the most unusual behaviors, including basal cell extrusions, motile multicellular protrusions, and hypermotile invasive cells, actually had lower total levels of activated Ras across the cell population than homogeneous MCF10A^{Ras} microtissues that only rarely manifested these phenotypes. Our results demonstrate that heterogeneity in pathway activation between neighboring cells is sufficient to drive emergent behaviors at the population level and highlight the need to control for the identity of surrounding cells when studying the effect of genetic, physical, or chemical perturbations applied at the single-cell level. More importantly, our results suggest that the regulation of cell-to-cell variability in Ras activation, particularly in developmental contexts, is important for controlling the global behavior of a tissue. Further investigation into the mechanisms by which cell-to-cell variability in Ras and other signaling pathways are maintained or suppressed in different biological contexts will provide greater insight into how tissue heterogeneity impacts multicellular behaviors.

EXPERIMENTAL PROCEDURES

Oligonucleotide Sequences

Oligonucleotide sequences are as follows:

A: 5'-linker-SH-ACTGACTGACTGACTGACTG-3'

B: 5'-linker-SH-CAGTCAGTCAGTCAGTCAGT-3'

Lipid DNA A: 5'-dialkyl-(T)₈₀-ACTGACTGACTGACTGACTG-3

Lipid DNA B: 5'-dialkyl-(T)₈₀-CAGTCAGTCAGTCAGTCAGT-3

General Materials and Reagents

Oligonucleotides were synthesized on an Expedite 8909 using standard phosphoramidite chemistry. Phosphoramidites were purchased from Glen Research and AZCO Biotech. Modified oligonucleotides were purified on an Agilent 1200 HPLC equipped with a semiprep Zorbax reversed phase C18 (oligos A and B) or semiprep Phenomenex C4 (Lipid DNA A and B) column and running a gradient of ACN in 0.1 M TEAA from 8% to 80%. Purified oligonucleotides were extensively lyophilized prior to use. NHS-modified DNA was prepared as previously described (Selden et al., 2012; Hsiao et al., 2009).

Antibodies, Growth Factors, and Inhibitors

The following antibodies were used for western blot: E-cadherin (BD Biosciences), tubulin (Sigma-Aldrich), phospho-Erk and phospho-Akt (Cell Signaling Technology), pan-Ras (Calbiochem), goat anti-mouse-HRP, and goat anti-rabbit-HRP (Thermo Scientific). The following antibodies were used for immunofluorescent staining: GM130, β -catenin (BD Biosciences), α 6-integrin, laminin-5 (Millipore), cleaved caspase-3 (Cell Signaling Technology), Ki-67 (Sigma-Aldrich), gp135 (a kind gift from Professor Keith Mostov), Alexa Fluor 488- and 568-conjugated goat anti-mouse, anti-rat, and anti-rabbit antibodies (Invitrogen). F-actin was stained with Alexa Fluor 488- or 568-conjugated phalloidin (Invitrogen). LY294002 and PD325901 (Calbiochem) were used at 20 μ M and 200 nM, respectively. TURBO DNase (Invitrogen) was used at a concentration of 10 U/ml.

Cell Lines and Cell Culture

MDCK cells were kindly provided by Professor Keith Mostov and cultured as previously described by Martin-Belmonte et al. (2007). MCF10A cells were kindly provided by Professor Jay Debnath (UCSF), and MCF10AneoT cells were obtained from the Karmanos Cancer Institute (Detroit). Both cell lines were cultured as previously described by Dawson et al. (1996) and Debnath et al. (2003). 3D on-top cultures were performed as previously described using growth factor-reduced IrECM lots with protein concentrations between 9 and 11 mg/ml (Matrigel; BD Biosciences) (Debnath et al., 2003). Cell lines expressing H2B-RFP proteins were prepared by transduction with lentivirus derived from pHIV-H2B-mRFP (Addgene; plasmid 18982) (Welm et al., 2008). H2B-eGFP was cloned from Addgene plasmid 11680 and ligated into pHIV to produce pHIV-eGFP (Kanda et al., 1998). Lentivirus was produced at the UCSF Sandler Lentiviral Core.

Cell Surface Labeling and Programmed Assembly

Cell surface labeling was performed as previously described by Selden et al. (2012). Cells were lifted by an incubation in 0.04% EDTA until cells rounded, followed by a 0.05% trypsin pulse. Trypsin was quenched by soybean trypsin inhibitor (Sigma-Aldrich). Cells were washed three times with base medium and then labeled with NHS-DNA for 30 min or with dialkylphosphoglyceride-DNA for 5 min at room temperature followed by three washes

with base medium. DNA-labeled cells were filtered through a 40 μm mesh, counted, mixed at greater than 1–50 ratios in polypropylene tubes, centrifuged, and gently resuspended. Aggregates were purified directly into eight-chamber slides containing 3D assay media using a FACSAriaII or FACSAriaIII (UCSF Laboratory for Cell Analysis) equipped with a 130 μm nozzle and a sheath pressure of 10 psi.

Microscopy

Time-lapse images of aggregates were acquired on a Zeiss 200M inverted fluorescence microscope equipped with an XCite argon light source and a Hamamatsu camera. Field positions were programmed into Slidebook 5.0 software, and images were acquired at 30 min intervals. Samples were maintained in a humidified chamber at 37°C and 5% CO₂. Phenotypes were scored in Slidebook 5.0 software after acquisition. Microtissues that merged with other microtissues or single cells were not scored due to confounding effects on cell motility.

Immunofluorescence Analysis and Image Acquisition

3D cultures were stained as previously described by Debnath et al. (2003). Confocal images were taken at the equatorial plane of the developing micro-tissues and were acquired on an inverted Zeiss LSM 510 NLO laser-scanning microscope (UCSF Laboratory for Cell Analysis). All imaged aggregates contained at least one GFP-labeled nucleus, although not necessarily in the plane of the confocal slice. Polarity, proliferation, and apoptosis counting were performed on a Nikon TiE inverted microscope equipped with a CSU-X1 confocal head. Channel intensities were adjusted linearly and equally across all images in each experiment using ImageJ and Adobe Photoshop software.

Supplementary Material

Refer to Web version on PubMed Central for supplementary material.

Acknowledgments

We thank Professors Mina Bissell, Jay Debnath, Keith Mostov, Jack Taunton, Kevan Shokat, and Pam England for many stimulating conversations and suggestions along with shared facilities and reagents. Lentiviruses were produced in the UCSF Viracore. Flow cytometry resources were provided by the UCSF Laboratory of Cell Analysis. We are grateful for support from DOD W81XWH-10-1-1023, NSF DGE-0648991, UCSF CTSI-SOS pilot grant 1 UL1 RR024131-01, the Program for Breakthrough Biological Research, grant 1RG9715010 from the American Cancer Society, a grant from the Sydney Kimmel Family Foundation, and grant P50 GM081879 to the UCSF Center for Systems and Synthetic Biology.

References

- Altschuler SJ, Wu LF. Cellular heterogeneity: Do differences make a Difference? *Cell*. 2010; 141:559–563. [PubMed: 20478246]
- Basolo F, Elliott J, Tait L, Chen XQ, Maloney T, Russo IH, Pauley R, Momiki S, Caamano J, Klein-Szanto AJ, et al. Transformation of human breast epithelial cells by c-Harar oncogene. *Mol Carcinog*. 1991; 4:25–35. [PubMed: 2009132]
- Dawson PJ, Wolman SR, Tait L, Heppner GH, Miller FR. MCF10AT: a model for the evolution of cancer from proliferative breast disease. *Am J Pathol*. 1996; 148:313–319. [PubMed: 8546221]
- Debnath J, Mills KR, Collins NL, Reginato MJ, Muthuswamy SK, Brugge JS. The role of apoptosis in creating and maintaining luminal space within normal and oncogene-expressing mammary acini. *Cell*. 2002; 111:29–40. [PubMed: 12372298]
- Debnath J, Muthuswamy SK, Brugge JS. Morphogenesis and oncogenesis of MCF-10A mammary epithelial acini grown in three-dimensional basement membrane cultures. *Methods*. 2003; 30:256–268. [PubMed: 12798140]

- Eisenhoffer GT, Loftus PD, Yoshigi M, Otsuna H, Chien CB, Morcos PA, Rosenblatt J. Crowding induces live cell extrusion to maintain homeostatic cell numbers in epithelia. *Nature*. 2012; 484:546–549. [PubMed: 22504183]
- Elenbaas B, Spirio L, Koerner F, Fleming MD, Zimonjic DB, Donaher JL, Popescu NC, Hahn WC, Weinberg RA. Human breast cancer cells generated by oncogenic transformation of primary mammary epithelial cells. *Genes Dev*. 2001; 15:50–65. [PubMed: 11156605]
- Ferrari A, Veligodskiy A, Berge U, Lucas MS, Kroschewski R. ROCK-mediated contractility, tight junctions and channels contribute to the conversion of a preapical patch into apical surface during isochoric lumen initiation. *J Cell Sci*. 2008; 121:3649–3663. [PubMed: 18946028]
- Friedl P, Locker J, Sahai E, Segall JE. Classifying collective cancer cell invasion. *Nat Cell Biol*. 2012; 14:777–783. [PubMed: 22854810]
- Gartner ZJ, Bertozzi CR. Programmed assembly of 3-dimensional microtissues with defined cellular connectivity. *Proc Natl Acad Sci USA*. 2009; 106:4606–4610. [PubMed: 19273855]
- Gjorevski N, Nelson CM. Integrated morphodynamic signalling of the mammary gland. *Nat Rev Mol Cell Biol*. 2011; 12:581–593. [PubMed: 21829222]
- Graupera M, Guillermet-Guibert J, Foukas LC, Phng LK, Cain RJ, Salpekar A, Pearce W, Meek S, Millan J, Cutillas PR, et al. Angio-genesis selectively requires the p110alpha isoform of PI3K to control endothelial cell migration. *Nature*. 2008; 453:662–666. [PubMed: 18449193]
- Hogan C, Dupré-Crochet S, Norman M, Kajita M, Zimmermann C, Pelling AE, Piddini E, Baena-López LA, Vincent JP, Itoh Y, et al. Characterization of the interface between normal and transformed epithelial cells. *Nat Cell Biol*. 2009; 11:460–467. [PubMed: 19287376]
- Hsiao SC, Shum BJ, Onoe H, Douglas ES, Gartner ZJ, Mathies RA, Bertozzi CR, Francis MB. Direct cell surface modification with DNA for the capture of primary cells and the investigation of myotube formation on defined patterns. *Langmuir*. 2009; 25:6985–6991. [PubMed: 19505164]
- Hüsemann Y, Geigl JB, Schubert F, Musiani P, Meyer M, Burghart E, Forni G, Eils R, Fehm T, Riethmüller G, Klein CA. Systemic spread is an early step in breast cancer. *Cancer Cell*. 2008; 13:58–68. [PubMed: 18167340]
- Inaki M, Vishnu S, Cliffe A, Rørth P. Effective guidance of collective migration based on differences in cell states. *Proc Natl Acad Sci USA*. 2012; 109:2027–2032. [PubMed: 22308382]
- Kajita M, Hogan C, Harris AR, Dupre-Crochet S, Itasaki N, Kawakami K, Charras G, Tada M, Fujita Y. Interaction with surrounding normal epithelial cells influences signalling pathways and behaviour of Src-transformed cells. *J Cell Sci*. 2010; 123:171–180. [PubMed: 20026643]
- Kanda T, Sullivan KF, Wahl GM. Histone-GFP fusion protein enables sensitive analysis of chromosome dynamics in living mammalian cells. *Curr Biol*. 1998; 8:377–385. [PubMed: 9545195]
- Khwaja A, Lehmann K, Marte BM, Downward J. Phosphoinositide 3-kinase induces scattering and tubulogenesis in epithelial cells through a novel pathway. *J Biol Chem*. 1998; 273:18793–18801. [PubMed: 9668053]
- Kim SH, Miller FR, Tait L, Zheng J, Novak RF. Proteomic and phosphoproteomic alterations in benign, premalignant and tumor human breast epithelial cells and xenograft lesions: biomarkers of progression. *Int J Cancer*. 2009; 124:2813–2828. [PubMed: 19291795]
- Leung CT, Brugge JS. Outgrowth of single oncogene-expressing cells from suppressive epithelial environments. *Nature*. 2012; 482:410–413. [PubMed: 22318515]
- Liu KD, Datta A, Yu W, Brakeman PR, Jou TS, Matthy MA, Mostov KE. Rac1 is required for reorientation of polarity and lumen formation through a PI 3-kinase-dependent pathway. *Am J Physiol Renal Physiol*. 2007; 293:F1633–F1640. [PubMed: 17804488]
- Lu P, Ewald AJ, Martin GR, Werb Z. Genetic mosaic analysis reveals FGF receptor 2 function in terminal end buds during mammary gland branching morphogenesis. *Dev Biol*. 2008; 321:77–87. [PubMed: 18585375]
- Marinari E, Mehonic A, Curran S, Gale J, Duke T, Baum B. Live-cell delamination counterbalances epithelial growth to limit tissue overcrowding. *Nature*. 2012; 484:542–545. [PubMed: 22504180]
- Martin-Belmonte F, Gassama A, Datta A, Yu W, Rescher U, Gerke V, Mostov K. PTEN-mediated apical segregation of phosphoinositides controls epithelial morphogenesis through Cdc42. *Cell*. 2007; 128:383–397. [PubMed: 17254974]

- Marusyk A, Almendro V, Polyak K. Intra-tumour heterogeneity: a looking glass for cancer? *Nat Rev Cancer*. 2012; 12:323–334. [PubMed: 22513401]
- Mori H, Gjorevski N, Inman JL, Bissell MJ, Nelson CM. Self-organization of engineered epithelial tubules by differential cellular motility. *Proc Natl Acad Sci USA*. 2009; 106:14890–14895. [PubMed: 19706461]
- O'Brien LE, Tang K, Kats ES, Schutz-Geschwender A, Lipschutz JH, Mostov KE. ERK and MMPs sequentially regulate distinct stages of epithelial tubule development. *Dev Cell*. 2004; 7:21–32. [PubMed: 15239951]
- Pearson GW, Hunter T. Real-time imaging reveals that non-invasive mammary epithelial acini can contain motile cells. *J Cell Biol*. 2007; 179:1555–1567. [PubMed: 18166657]
- Pearson GW, Hunter T. PI-3 kinase activity is necessary for ERK1/2-induced disruption of mammary epithelial architecture. *Breast Cancer Res*. 2009; 11:R29. [PubMed: 19457236]
- Rhim AD, Mirek ET, Aiello NM, Maitra A, Bailey JM, McAllister F, Reichert M, Beatty GL, Rustgi AK, Vonderheide RH, et al. EMT and dissemination precede pancreatic tumor formation. *Cell*. 2012; 148:349–361. [PubMed: 22265420]
- Rosenblatt J, Raff MC, Cramer LP. An epithelial cell destined for apoptosis signals its neighbors to extrude it by an actin- and myosin-dependent mechanism. *Curr Biol*. 2001; 11:1847–1857. [PubMed: 11728307]
- Scott RW, Hooper S, Crighton D, Li A, König I, Munro J, Trivier E, Wickman G, Morin P, Croft DR, et al. LIM kinases are required for invasive path generation by tumor and tumor-associated stromal cells. *J Cell Biol*. 2010; 191:169–185. [PubMed: 20876278]
- Selden NS, Todhunter ME, Jee NY, Liu JS, Broaders KE, Gartner ZJ. Chemically programmed cell adhesion with membrane-anchored oligonucleotides. *J Am Chem Soc*. 2012; 134:765–768. [PubMed: 22176556]
- Shen J, Dahmann C. Extrusion of cells with inappropriate Dpp signaling from *Drosophila* wing disc epithelia. *Science*. 2005; 307:1789–1790. [PubMed: 15774763]
- Slattum G, McGee KM, Rosenblatt J. P115 RhoGEF and microtubules decide the direction apoptotic cells extrude from an epithelium. *J Cell Biol*. 2009; 186:693–702. [PubMed: 19720875]
- Streuli CH, Bailey N, Bissell MJ. Control of mammary epithelial differentiation: basement membrane induces tissue-specific gene expression in the absence of cell-cell interaction and morphological polarity. *J Cell Biol*. 1991; 115:1383–1395. [PubMed: 1955479]
- Takemura M, Adachi-Yamada T. Repair responses to abnormalities in morphogen activity gradient. *Dev Growth Differ*. 2011; 53:161–167. [PubMed: 21338342]
- Tanner K, Mori H, Mroue R, Bruni-Cardoso A, Bissell MJ. Coherent angular motion in the establishment of multicellular architecture of glandular tissues. *Proc Natl Acad Sci USA*. 2012; 109:1973–1978. [PubMed: 22308439]
- Vitorino P, Meyer T. Modular control of endothelial sheet migration. *Genes Dev*. 2008; 22:3268–3281. [PubMed: 19056882]
- Wang X, He L, Wu YI, Hahn KM, Montell DJ. Light-mediated activation reveals a key role for Rac in collective guidance of cell movement in vivo. *Nat Cell Biol*. 2010; 12:591–597. [PubMed: 20473296]
- Weinberg RA. Leaving home early: reexamination of the canonical models of tumor progression. *Cancer Cell*. 2008; 14:283–284. [PubMed: 18835030]
- Welm BE, Dijkgraaf GJ, Bledau AS, Welm AL, Werb Z. Lentiviral transduction of mammary stem cells for analysis of gene function during development and cancer. *Cell Stem Cell*. 2008; 2:90–102. [PubMed: 18371425]
- Yuan TL, Wulf G, Burga L, Cantley LC. Cell-to-cell variability in PI3K protein level regulates PI3K-AKT pathway activity in cell populations. *Curr Biol*. 2011; 21:173–183. [PubMed: 21256021]

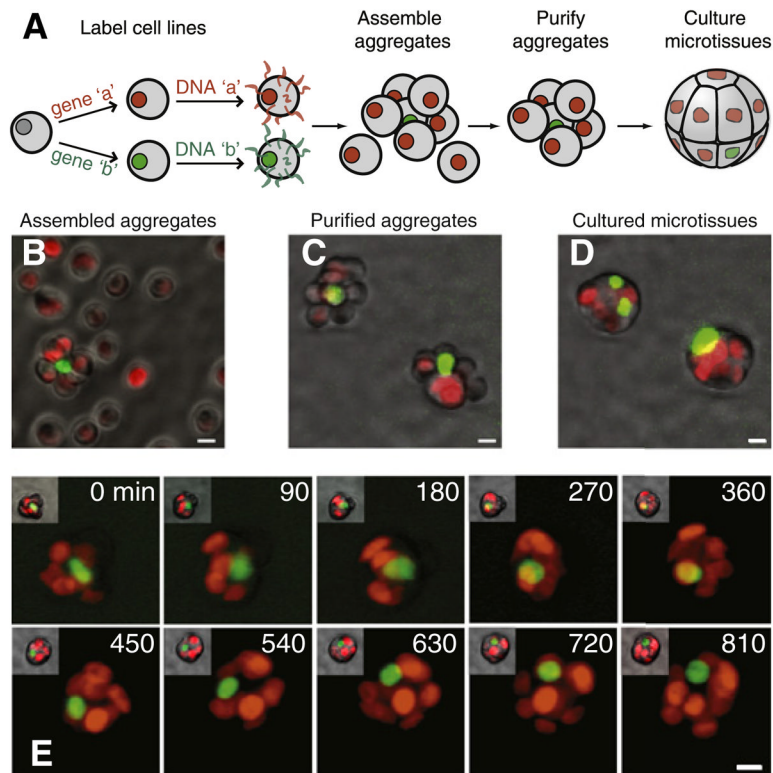


Figure 1. Programming the Assembly of Mosaic Epithelial Aggregates of Defined Size, Composition, and Initial Cell-to-Cell Connectivity

(A) Scheme for the programmed assembly of mosaic epithelial microtissues.

(B) Single H2B-GFP-expressing MCF10A cells assembled 1:50 with H2B-RFP-expressing MCF10A cells.

(C) Aggregates after purification by FACS.

(D) MCF10A aggregates as shown in (C) condensed into rounded microtissues after 8.5 hr culture in IrECM.

(E) Time series from Movie S1 showing motion of fluorescently labeled nuclei during condensation of an aggregate (insets) into a microtissue.

Scale bars, 10 μm . See also Figure S1.

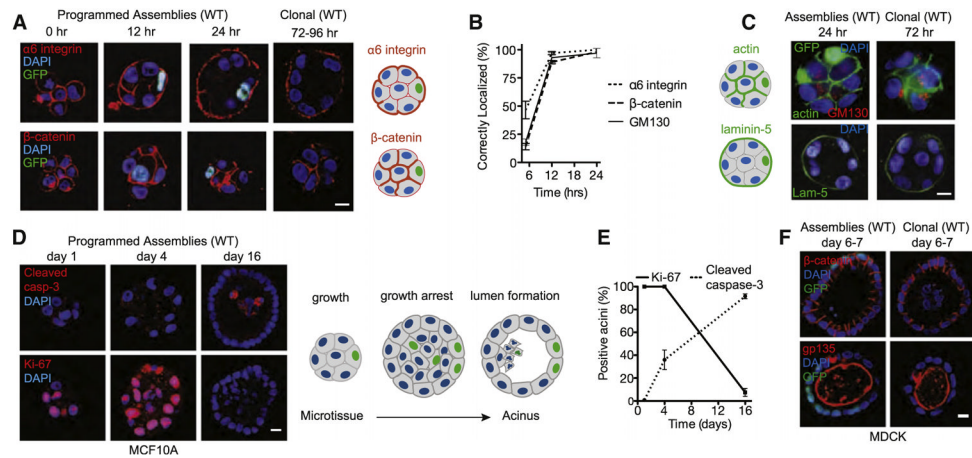


Figure 2. Onset of Polarity, Growth Arrest, and Lumen Formation in MCF10A Cell Aggregates

(A) Representative confocal immunofluorescence images of MCF10A aggregates stained for α_6 -integrin and β -catenin after 0, 12, and 24 hr in 3D culture, and representative immunofluorescence images of similarly sized microtissues grown from single cells for comparison. A schematic illustrating the correct localization of α_6 -integrin and β -catenin for MCF10A microtissues undergoing morphogenesis is shown to the right.

(B) Quantification of the onset of polarity in assembled aggregates of MCF10A^{WT} cells. Values are means with error bars representing the SDs of the mean of 60 observations from at least two independent replicates.

(C) Representative confocal immunofluorescence images of assembled MCF10A aggregates indicating correct localization of basement membrane component laminin-5 and cytoskeletal component F-actin after 24 hr in 3D culture.

(D) Representative confocal immunofluorescence images of assembled MCF10A aggregates stained for cleaved caspase-3 and Ki-67 after 1, 4, and 16 days in culture (left). Schematic of MCF10A microtissue proliferation, growth arrest, and lumen formation (right).

(E) Quantification of growth arrest and apoptotic lumen formation in microtissues grown from MCF10A aggregates. Data are expressed as the mean, and error bars represent the SD of the mean from at least two independent experiments (n = 60).

(F) MDCK aggregates and similarly sized cysts grown from single cells stained for basolateral marker β -catenin and apical marker gp135 after 6 or 7 days. Scale bars, 10 μ m. See also Figure S2.

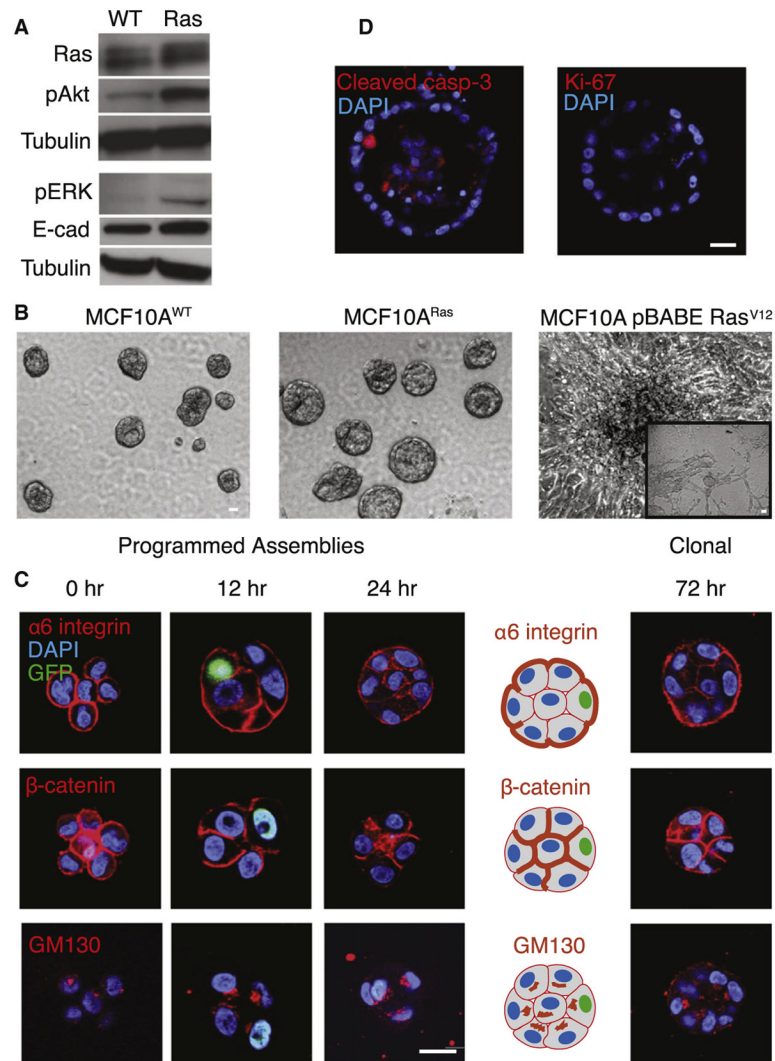


Figure 3. Assembled MCF10A^{Ras} Cells Undergo Morphogenesis Similar to MCF10A WT Cells
 (A) Western blots for Ras, phospho-Akt, phospho-Erk, and E-cadherin (E-cad) for MCF10A^{WT} and MCF10A^{Ras} cells.

(B) Phase-contrast images of MCF10A^{WT}, MCF10A^{Ras}, and pBabe-puro Ras^{V12}-transduced MCF10A cells cultured for 23 days in lrECM. Inset shows the pBabe-puro Ras^{V12}-transduced cells after 5 days of culture in lrECM.

(C) Representative confocal immunofluorescence images of homogeneous MCF10A^{Ras} cell aggregates stained for polarity and adherens junction proteins after culture in lrECM for the indicated times. These images should be compared to representative immunofluorescence images of similarly sized microtissues grown from single cells (right) and MCF10A^{WT}-staining patterns as shown in Figures 2A and S2A.

(D) Representative confocal immunofluorescent images of homogeneous MCF10A^{Ras} aggregates stained for cleaved caspase-3 and Ki-67 after 16 or more days in culture. Scale bars, 20 μ m. See also Figure S2.

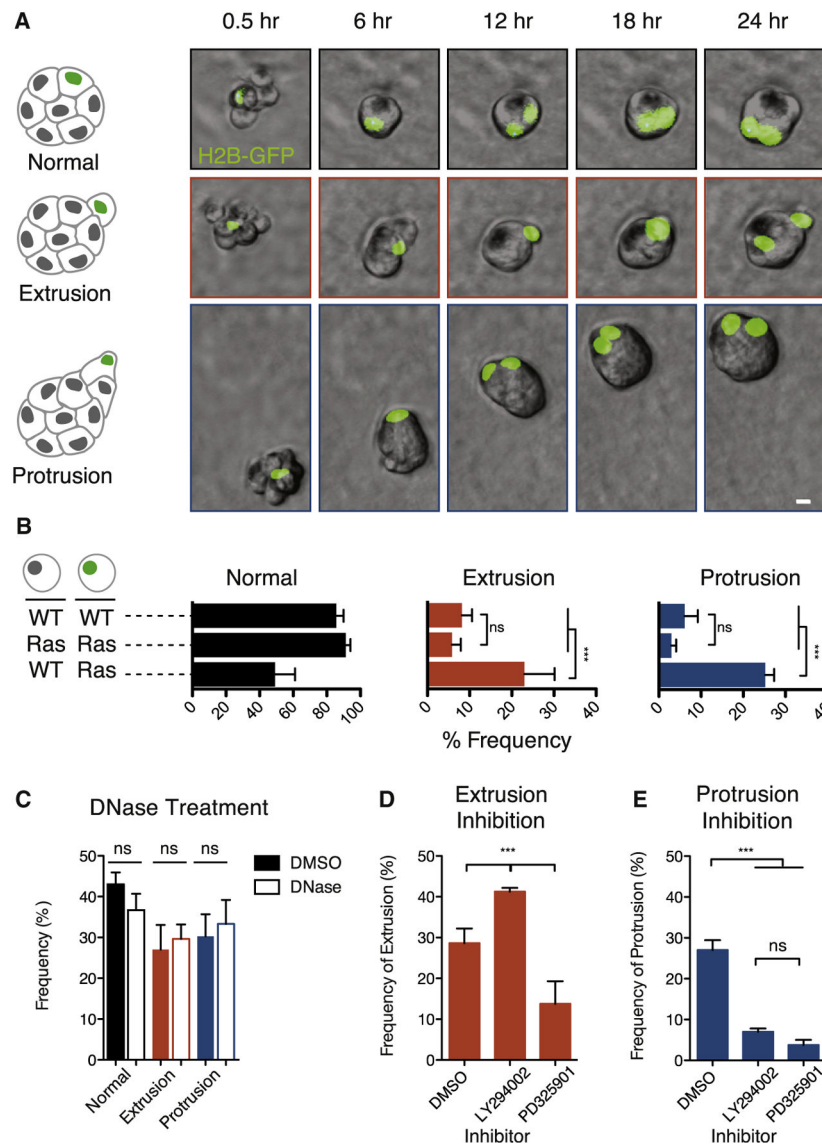


Figure 4. Emergent Behaviors in Microtissues Heterogeneous for Signaling Downstream of H-Ras

(A) Representative time-lapse images from Movie S4 showing normal and emergent phenotypes in the mosaic MCF10A^{Ras}/MCF10A^{WT} microtissues.

(B) Quantification of normal, basal cell extrusion, and motile multicellular protrusion frequency in homogeneous and heterogeneous microtissues. Data are expressed as the mean of at least 700 observations from four independent experiments, and error bars represent the SD of the mean.

(C) Sensitivity of the frequency of emergent phenotypes to the addition of high-activity DNase immediately after assembly.

(D) Sensitivity of cell extrusion and (E) motile multicellular protrusions to inhibition of PI3K by LY294002 and MEK by PD325901. Values are the averages of at least 400 total events from three independent experiments, and error bars show the SD of the means.

Scale bar, 20 μ m. *** $p < 0.001$; ns, not significant (one-way ANOVA and Tukey's test). See also Figure S3.

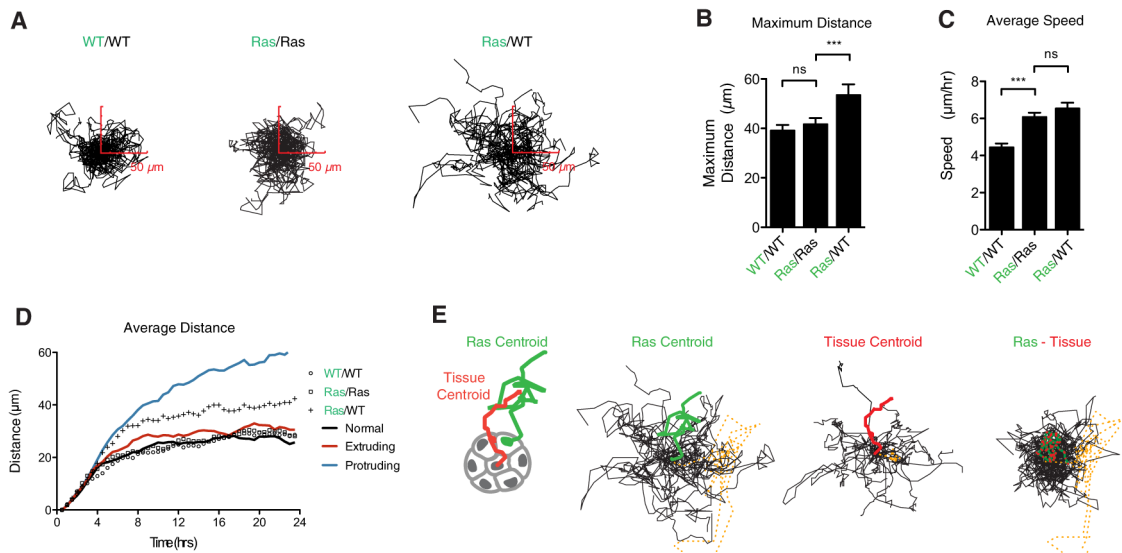


Figure 5. Quantitative Analysis of Cell Motility during Emergent Behaviors

(A) A total of 30 superimposed 24 hr trajectories for cells expressing H2B-GFP fusions growing in homogeneous and heterogeneous MCF10A^{Ras}/MCF10A^{WT} microtissues of the indicated composition.

(B) Average maximum distance traveled and (C) speed of the H2B-GFP-expressing cell under the conditions in (A).

(D) Average distance traveled as a function of time for H2B-GFP-expressing cell in either homogeneous or heterogeneous microtissues. Average distances for H2B-GFP-expressing cells in heterogeneous microtissues are broken down into normal, motile multicellular protrusion, and basal extrusion phenotypes.

(E) Trajectories of H2B-GFP-expressing MCF10A^{Ras} cells and the centroid of the surrounding WT microtissue. Microtissue trajectories (center) are subtracted from MCF10A^{Ras} trajectories (left) to produce the residual trajectories (right). A representative MCF10A^{Ras} cell (green), associated microtissue (red), and residual trajectory (hatched green and red) are highlighted. Trajectory of a hypermotile cell leaves a large residual (dashed orange lines).

For (B) and (C), values are expressed as the mean with SD of 525 observations for three replicate experiments. For (A), (D), and (E), data are shown from a single experiment that is representative of three replicates. Trajectories are bounded by a 100 μm radius.

See also Figure S4.